Master's Thesis

Pattern reconfigurable MIMO antennas for Multiband LTE Operation

Rui Ma
Ioannis Chountalas

Master's Thesis

Pattern reconfigurable MIMO antennas for Multiband LTE Operation

By

Rui Ma and Ioannis Chountalas

Department of Electrical and Information Technology
Faculty of Engineering, LTH, Lund University
SE-221 00 Lund, Sweden

Abstract

Nowadays, multiple antennas are becoming widely used in small mobile terminals as they can significantly improve wireless communication performance in terms of link reliability and spectral efficiency. Also, pattern reconfiguration is another new trend for antenna design as it enables the antennas to adapt to different propagation and user scenarios. However, due to the limited space in the terminals, it is difficult to implement both techniques and obtain good antenna performance, especially for frequency bands below 1 GHz. This is because the mobile chassis is often shared by different antennas as the main radiator, regardless of the antenna structure, which leads to high mutual coupling and correlation.

In this thesis, a dual-band (824-894 MHz and 1850-1990 MHz) MIMO antenna system with pattern reconfiguration at the low band was designed based on the theory of characteristic modes (TCM). The work began with the design of a single reconfigurable antenna that can be switched between an inverted-F antenna (IFA) mode and a bezel mode, with low envelope correlation of around 0.2 between the states. This was followed by the implementation of a second antenna (i.e., a single-side T-strip) for MIMO operation. The inclusion of the second antenna required the antenna system to be re-optimized, and several performance trade-offs were observed and investigated, including the tradeoff in the mutual coupling between the MIMO antennas in different states as well as the tradeoff between the mutual coupling and the inter-state correlation. The final design of the pattern reconfigurable MIMO antennas yields an inter-state correlation of around 0.3, and an intra-state correlation of below 0.1 and 0.2, respectively. All the studies were carried out in CST Microwave Studio and Matlab.

Acknowledgments

Table of Contents

Preface

The responsibility of performing this thesis project is divided between Rui and Ioannis in the following way: For Chapter 1, Ioannis wrote the introduction, literature review, thesis objectives and organization, whereas Rui wrote the description of reconfigurable antennas, mutual coupling and Envelope Correlation Coefficient (ECC). For Chapter 2, Ioannis performed the background research on the Theory of Characteristic Modes (TCM) and used it to analyze several modified chassis structures. Rui provided the introductions of several antennas (i.e., common mobile antennas, bezel antenna, inverted-F antenna (IFA), slot antenna, T-strip antenna) for Chapter 3. For the simulations in Chapter 4, both Rui and Ioannis took active roles in designing the whole antenna structure in the Frequency Domain Solver of CST Microwave Studio. Rui mostly worked on the IFA/bezel antenna part whereas Ioannis focused on the T-strip antenna part. For Chapter 5, the work was also divided into two parts, Rui performed the discussion on the trade-offs of mutual couplings in the two reconfigurable states. Ioannis dealt with the final simulation results and the comparison between the simulated antenna radiation patterns and the eigenmode radiation patterns. Finally, the responsibility for writing the conclusion and future work in Chapters 6 and 7 was taken by Rui.

CHAPTER 1

1 Introduction

Multiple-Input Multiple-output (MIMO) refers to the system in which two or more antennas are used in both the transmitter and receiver. It is widely used in wireless communications, specifically in mobile communications after its implementation in 2010 with the release of Long Term Evolution (LTE). In a MIMO system, apart from the frequency-time domain along with code-based technologies, the dimension of space is also put into use. This enables us to achieve greater spectral efficiency, equivalently higher data rates for a certain bandwidth, or better quality-of-service through techniques such as beamforming, diversity or spatial multiplexing.

To take advantage of MIMO system, mobile phones are required to have two or more antennas at the same frequency bands. According to the LTE standard, multiple antennas in the mobile handsets are used for downlink only, with uplink working with only one transmitting antenna. With the release of LTE Advanced (LTE-A) in 2013 onwards, antennas in the mobile handsets are used for the uplink as well. This change called for improvement on the antennas which in turn increases complexity and design difficulties in the already cramped chassis of an LTE capable smartphone. For example due to construction characteristics and restrictions, the whole chassis structure serves as the main radiator resulting in severe coupling among the antennas.

This thesis investigates the challenging task of designing a reconfigurable antenna and implementing it in a MIMO system as part of a LTE mobile handset. Antenna design is carried out with the help of the Theory of Characteristic Modes (TCM). It is shown that additional current modes can be created and excited by appropriately modifying the chassis. The TCM study was carried out in Matlab in order to find possible feeding locations of antennas, and verifications were performed on full-wave simulation software Computer Simulation Technology (CST) Microwave Studio.

1.1 Literature Review

Antenna reconfigurability in mobile handsets has been investigated mainly with respect to frequency reconfiguration. Elfergani et al. in [1] and Lee et al. in [2] gave examples of frequency reconfigurable antennas on mobile handsets with their focus on frequencies bands above 1 GHz. In [3], Elfergani et al. propose a harmonic suppression technique for reconfigurable antennas for mobile applications. Pattern reconfigurable antennas with use of TCM in mobile handsets are seen in Kishor's work in [4] and [5], but again, there is no investigation for the bands below 1 GHz.

In [6] Garbacz et al. presented a generalized expansion for radiated scattered fields. In [7] Harrington investigated it and refined it further, resulting in a more approachable and computationally applicable formulation called TCM. TCM was later expanded to include dielectric materials as well [8].

In the application domain, TCM was firstly used as an antenna shaping tool [9] but with the advancement of computers and the increase of computational power there has been a growing interest of using it as a tool for estimating radiation fields of arbitrarily shaped conducting and non-conducting structures.

TCM provides guidelines for the design of multiple antennas with small correlation on the same devices. This is accomplished by exciting different characteristic modes of the chassis [10], [11]. In [12], TCM was applied to a MIMO handset to design uncorrelated antennas by using a feeding point between a metal back cover on the chassis and the ground plane of the handset. In [13] Krewski et al. use TCM to excite different modes by symmetrically placing couplers on a laptop chassis. Similarly, in [14] Manteuffel and Martens use couplers to excite different current modes for a compact design.

In [15] and [16] TCM was applied on handset terminals with bezel-type and T-strip antennas respectively, to enable MIMO antenna design in frequency bands below 1 GHz. This thesis extends on the work in [15] and [16] by implementing the reconfigurability aspect into these previous designs.

1.2 Thesis Objectives and Organization

In this thesis, a dual-band (824-894 MHz and 1850-1990 MHz) MIMO antenna system with pattern reconfiguration at the low band was designed

based on TCM. The work started with the design of a single, pattern-reconfigurable antenna that can be switched between two modes: an inverted-F antenna (IFA) mode and a bezel mode. The goal is to achieve low envelope correlation (ρ), of around 0.2 between the two states. After that, a T-strip antenna is implemented on the opposite side of the chassis for MIMO operation. The inclusion of the T-strip antenna required the reconfigurable antenna to be re-optimized, and several performance trade-offs were observed and investigated.

Briefly, when the complete structure was brought together, the mutual coupling of the antenna configurations was not yielding the expected results. For example the IFA state of operation was yielding a result of -5dB in the coupling coefficient (S_{12}) parameter (approximately 30% of radiated energy is coupled to the T-strip antenna). This is an unacceptable result, thus re-optimization of the complete structure had to take place.

Since the chassis layout did not offer many options for position re-arranging, a flip of the T-strip wing was implemented as a means for de-coupling the IFA state and the T-strip antenna which in turn had an impact on the bezel state performance. Several methods were tested at this point. Eventually the addition of an extra wing under the main IFA wing was decided as it yielded the most balanced results in between the states.

The current report firstly introduces the concepts and metrics that are widely used throughout this work. In Chapter 2, a detailed overview of TCM is presented, followed by the description of the antenna configurations implemented in Chapter 3. In Chapter 4, a detailed flow of work carried out in this thesis is presented, followed by the presentation of the achieved results in Chapter 5 and the conclusions and future work in Chapter 6.

1.3 Reconfigurable Antennas

Reconfigurable antennas are the kind of antennas which could modify dynamically their frequency, polarization or radiation properties in a controlled and reversible manner [17]. As shown in Fig. 1.1, in order to reconfigure the antennas, methods like RF switches, mechanical actuators or tunable materials, can be used [18]. The advantage of a pattern reconfigurable antenna lies in that it can switch between patterns to achieve high gain for the signal and suppress the interference. This makes the wireless communication link more reliable, or equivalently supporting

higher data rate. In order to obtain efficient reconfigurability, antenna patterns for different states should have very low correlation.
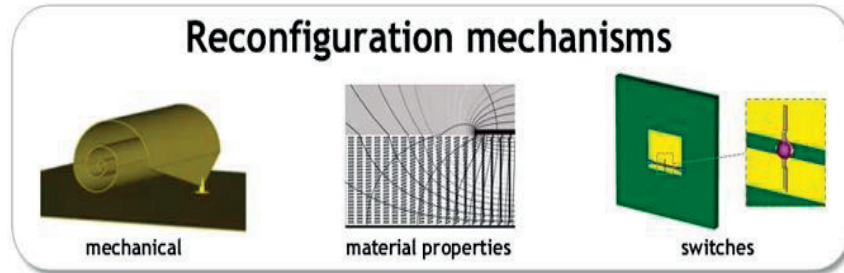

Fig. 1.1: Methods of realizing reconfiguration

In this thesis, reconfiguration of the radiation pattern is realized only in the low frequency range. The reconfigurable antenna is designed to switch between the IFA mode and bezel mode, which should have similar physical structures. The reconfiguration is performed through PIN diodes, and these two states are resonant at the same frequency band, but with different radiation patterns. With this reconfiguration, the desired mobile antennas could automatically adjust its pattern according to the environment to give better communication performance.

One thing to highlight is that, there are significant difficulties to achieve pattern reconfigurability in the low frequency range (below 1 GHz). According to [7], typical rectangular mobile chassis only provides one resonant characteristic mode in this frequency range. So generally without any modification of the chassis, only one radiation pattern could be produced. In this thesis, three modes are produced by adding a metal bezel and a T-strip on the chassis, which helps to realize pattern reconfiguration.

1.4 Mutual Coupling and Envelope Correlation Coefficient (ECC)

For multiple antenna design in a real handset, due to the limited size of the chassis, mutual coupling between the antennas is an inevitable problem. Mutual coupling is the electromagnetic interaction between antenna elements in multi-antennas. If two radiating antennas are relatively close to each other, current on one antenna will create electromagnetic (EM) field and the EM field induces current on another antenna exposed to that field. As a result, EM energy is transferred from the first antenna to the second

one. In this case, energy is wasted in the MIMO system, leading to lower antenna efficiency and thus lower data rate.

Envelope correlation coefficient (ECC) is another critical figure of merit which is influenced by mutual coupling. It describes how the signals received by the antennas are correlated. Higher correlation can lead to lower diversity gain and channel capacity.

Far-field patterns with magnitude and phase information can be presented in 3D spherical coordinates. Based on the patterns of two antennas, the calculation of ECC can be summarized as (1), (2) according to [19]:

$$\rho_e = \frac{\left|\iint_{4\pi} d\Omega F_1(\theta,\phi)^* \cdot F_2(\theta,\phi)\right|^2}{\iint_{4\pi} d\Omega |F_1(\theta,\phi)|^2 \iint_{4\pi} d\Omega |F_2(\theta,\phi)|^2} \tag{1}$$

$$F_i(\theta,\phi) = F_\theta^i(\theta,\phi)\hat{a}_\theta + F_\phi^i(\theta,\phi)\hat{a}_\phi \tag{2}$$

For a 3D uniform environment, ECC is equivalent to the pattern correlation between the antennas. In general, the correlation value ranges from 0 (best MIMO gain) to 1(worst MIMO gain). In the thesis, the radiation patterns with both amplitude and phase information were calculated from full-wave CST simulations, and Matlab codes were used to get the ECC values at each frequency.

In this thesis, the reconfigurable antenna works in two states, i.e., IFA state and bezel state. In the IFA state, an IFA antenna as well as a T-strip antenna is working at the same time. On the other hand, in the bezel state, a bezel antenna as well as a T-strip antenna is working instantaneously. Thus, ECC calculations were needed for both conditions: 1) between the MIMO antennas, which is named as "inter-state" correlation, and 2) between the two reconfiguration states, which is named as "intra-state" correlation.

Mutual coupling and correlation increased the difficulty in designing the MIMO antennas and the reconfigurable antenna. Some of the trade-offs in performance will be discussed later.

2 Background and Analysis of TCM

2.1 Theory of Characteristic Modes (TCM)

The Theory of Characteristic Modes (TCM) was firstly developed by Garbacz [6] and refined by Harrington and Mautz [7] at a later date. The theory is based on the eigenfunction expansion method, on which the current induced on the conductive surface is represented as weighted sums of eigenfunctions. According to TCM, at a certain frequency, every arbitrarily shaped conducting structure has a particular set of surface currents and corresponding radiated fields, which are characteristic of that shape of structure, and independent of particular excitation. So by definition, characteristic modes are current modes calculated for a conducting surface at a specific frequency. These currents are defined as the eigenfunctions of the eigenvalue equation that involves the impedance matrix of the surface under investigation and are obtained as the eigenfunctions of the following particular weighted eigenvalue in (3) based on [10]:

$$X(\vec{J}_n) = \lambda_n R(\vec{J}_n) \tag{3}$$

where λ_n are the eigenvalues, the $\vec{J}_n$ are the eigencurrents, R are the real parts of the impedance and X are the imaginary parts of the impedance.

The orthogonality of the modes derives from the relation of the power P associated with the different modes and is implied by the Kronecker's delta function δ_{mn} as shown in (4). By definition, the characteristic impedance is in the form $Z = R + jX$ and it consists of a real and a reactive part associated with the radiated and stored energy [14]:

$$P(J_m, J_n) = \left\langle \overrightarrow{J_m^*}, Z(\vec{J_n}) \right\rangle = \langle J_m^*, RJ_n \rangle + j \langle J_m^*, XJ_n \rangle$$

$$= \underbrace{\oiint_{S'} E_m \times H_n^* dS'}_{\delta_{mn}} + \underbrace{j\omega \iiint_{V'} (\mu H_m \cdot H_n^* - \varepsilon E_m \cdot E_n^*)dV}_{j\lambda_n \delta_{mn}}$$

$$= (1 + j\lambda_n)\delta_{mn}$$

$$(4)$$

In all the following figures presented in this chapter, the eigenmodes touching/crossing the value of 0 on the x axis are the ones corresponding to the resonant frequencies of the structure. The bandwidth of the resonance is indicated from the slope of the curve.

The use of TCM is a promising tool for mobile antenna design, since it provides a more physical interpretation of the electromagnetic phenomena taking place on the chassis and radiating elements. Furthermore the fact that the characteristic modes are independent of excitation means that the optimization of the shape of the antennas/radiating elements can be fine-tuned separately from any matching feed. Scaling up/down the size of a radiating element will change the resonant frequencies of the modes, whereas making changes to the chassis will also affect the radiation pattern of the element [10].

2.2 TCM Analysis of Modified Chassis Structures

In this thesis, based on the result presented by Li et al. [20], several possible ways to feed a typically sized 4G mobile handset chassis with two ports is investigated, in such a way that radiation pattern reconfigurability, with low mutual coupling between the feeding ports as well as low correlation coefficient between the reconfigurable modes of the antenna, is achieved. The use of TCM is focused on the investigation of introducing new characteristic modes by altering the shape of the chassis, with the addition of a T-strip antenna and a bezel. The TCM study is also used to find the appropriate location of the feeding ports for the IFA reconfigurable setup.

First, a simple rectangular plate with the dimensions of 130 mm×65 mm ×0.1 mm (length, width, thickness respectively) is investigated. The eigenmodes of the plate over frequency is shown in Fig. 2.1. It is observed that there exists one characteristic mode (CM) at 1 GHz. The eigencurrents of the first mode of the structure is shown in Fig. 2.2, which presents an

electric dipole like pattern. In this work, this means that the basis of construction, the chassis, has a CM which can be excited as a radiating element. Since the interest of this thesis lies in MIMO as well as pattern reconfigurability, more than one mode is needed to achieve low correlation between antennas and between different pattern states. Thus, changes on the shape of the chassis were made, with the purpose of introducing additional CMs.
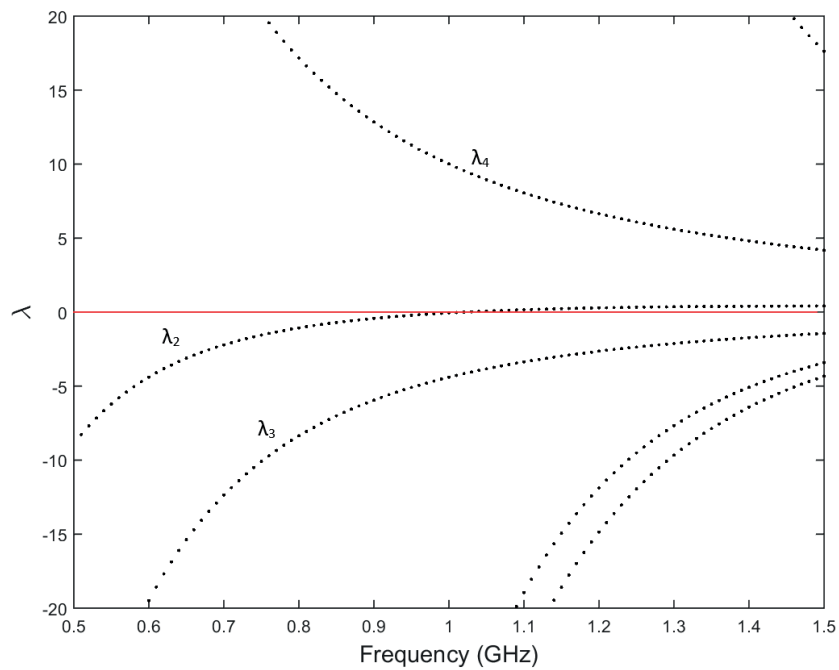

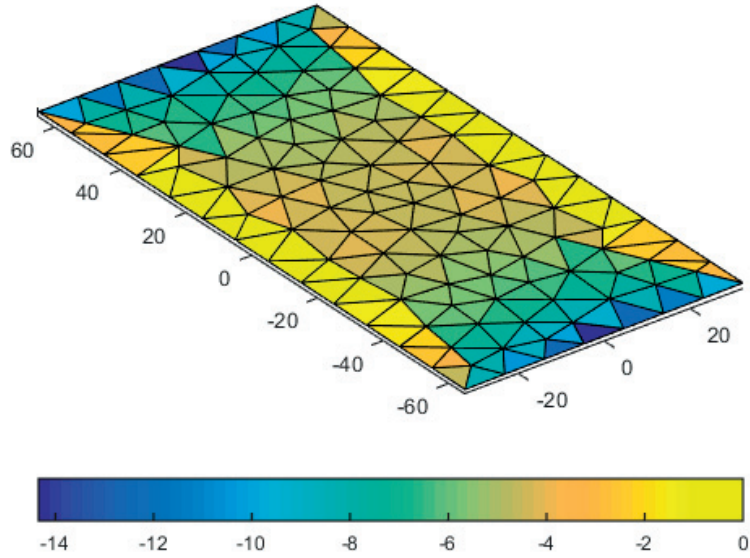Fig. 2.1: Eigenmodes of a rectangular plate from 0.5 GHz to 1.5 GHz

Fig. 2.2: Surface eigencurrents of a rectangular plate at 1 GHz for mode 2

According to [15], the addition of a bezel along the perimeter of a rectangular plate can introduce one additional CM below or close to 1 GHz which suits the purpose of this thesis. However, since this work aims at designing MIMO handset antennas, the use of the whole perimeter excludes the possibility to design additional antennas on the chassis, as there is no room left for the second antenna. Since the bezel resonates at one full wave length when it is not connected to the ground plane, the total length of the bezel can be reduced by half through connecting the bezel with two shorting pins, as shown in Fig. 2.3. The eigenvalues of the bezel loaded chassis is shown in Fig. 2.4. It is observed that besides the chassis mode (λ_5), whose curve is similar as in Fig. 2.2, a new mode (λ_4) is created, which is called the bezel mode in this thesis. The slope of the new mode is larger than that of the chassis mode, indicating a narrow bandwidth of the bezel mode. The surface eigencurrents of λ_4 for the half bezel loaded chassis is shown in Fig. 2.3. It is noteworthy that even though there is still no certain way to track the CMs of a structure, it is safe to assume that the mode coming from the rectangular plane provides an eigenvalue of similar curvature as before with a slight change in resonance and a small increase in the slope close to the zero crossing, which means a decrease of bandwidth in the case of that particular mode being excited.
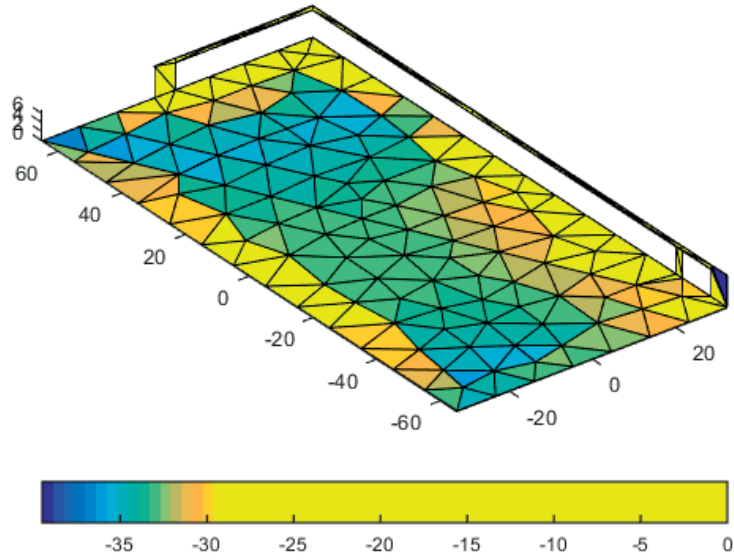
15

Fig. 2.3: Surface eigencurrents of a rectangular plate with a half-bezel antenna at 0.81 GHz
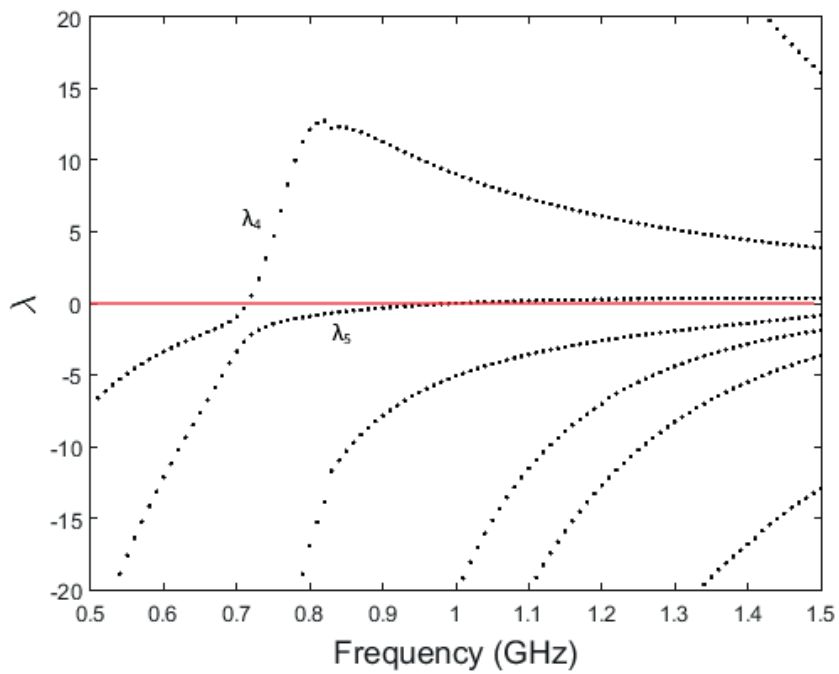for mode 4

Fig. 2.4: Eigenmodes of a rectangular plate with a half-bezel type structure

Another kind of chassis modification is T-strip loading. Different from [20], the T-strip is only loaded on one side of the chassis in this work. Similar results as in [20] were obtained when TCM analysis was performed on the aforementioned rectangular plate with the addition of a T-strip on one of the long sides (new structure shown in Fig. 2.5). As expected, a new CM is introduced (i.e., λ_5 in Fig. 2.6), along with that of the fundamental mode (λ_6). In Fig. 2.5 the surface eigencurrents for λ_5 are presented. In Fig. 2.6, the eigenvalues of these two CMs can be seen, with the fundamental mode [20] resulting from the length of the rectangular plate, and the T-strip mode (resonating at a lower frequency) resulting from the capacitively loaded width of the plate.
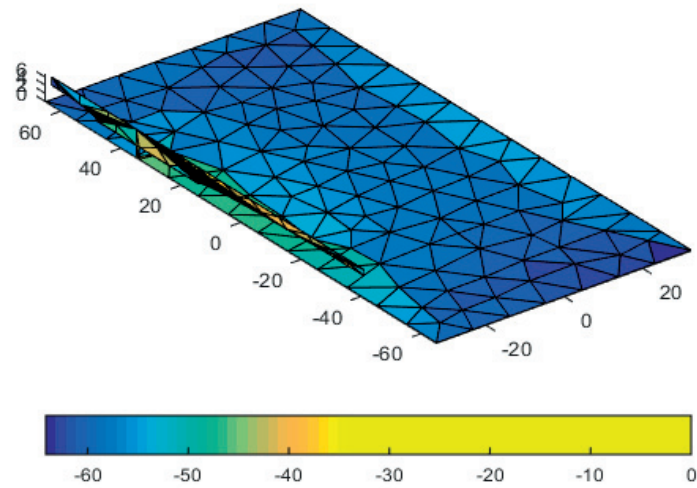

Fig. 2.5: Surface eigencurrents of a rectangular plate with a T-strip structure at 0.97 GHz for mode 5
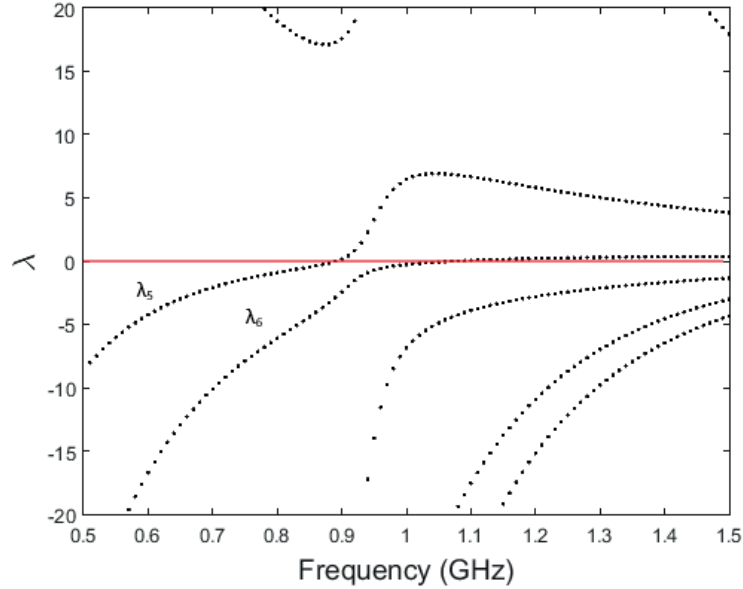
17

Fig. 2.6: Eigenmodes of a rectangular plate with a T-strip structure

Lastly, the modes of the chassis loaded by both the T-strip and the half-bezel (new structure shown in Fig. 2.7) are investigated. Some changes were made on the half-bezel shown in Fig. 2.7 due to the later concern of pattern configurability. As expected, three resonant CMs appear below 1 GHz for this structure, corresponding to the fundamental chassis mode (λ_6), bezel mode (λ_5) and T-strip mode (λ_4), respectively. The eigencurrents of the complete design are presented in Fig. 2.7, Fig. 2.8, and Fig. 2.9, whereas the eigenvalues of the eigenmodes are shown in Fig. 2.10. It is observed that there exist different eigencurrents that correspond to the different modes. One important thing to note is that even though the eigenmodes are perfectly orthogonal in theory, it is difficult in practice to design antenna feeds to selectively excite the individual modes with the corresponding eigencurrents. Therefore, some loss of orthogonality can be expected in practical multi-antenna design based on the excitation of multiple CMs at a given frequency.
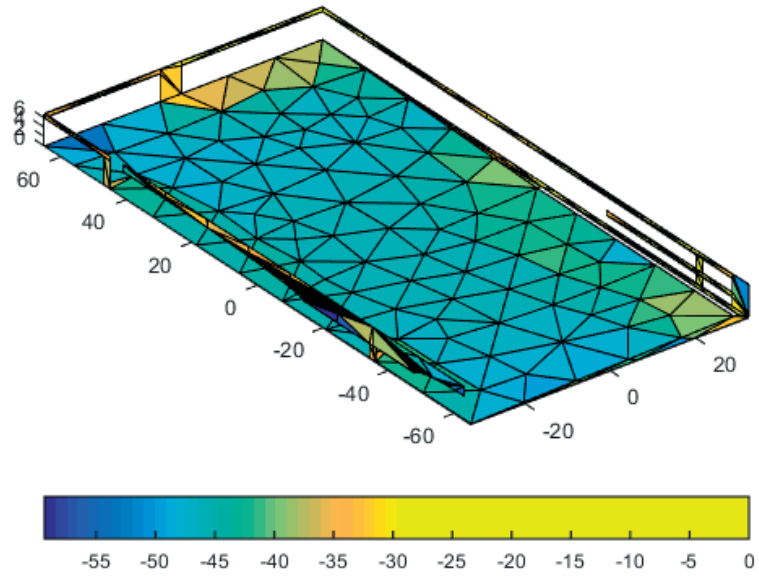
18

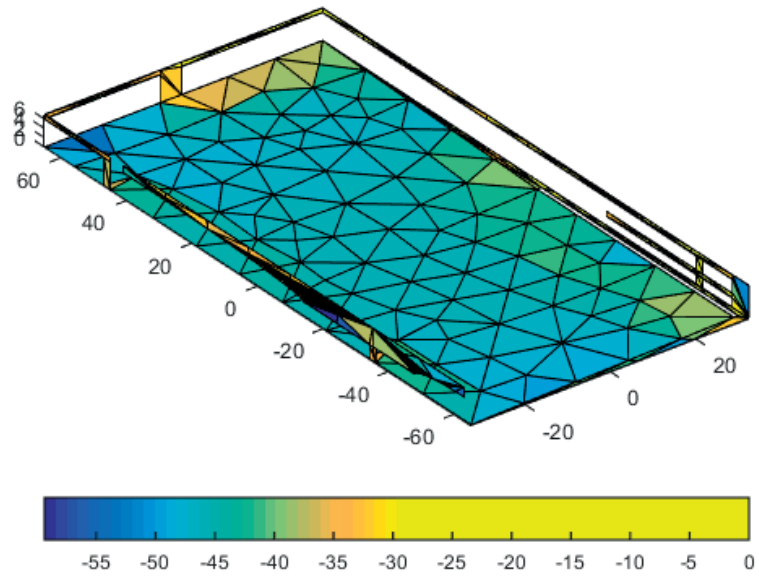Fig. 2.7: Surface eigencurrents of the full structure at 1 GHz for mode 4

Fig. 2.8: Surface eigencurrents of the full structure at 0.81 GHz for mode 6
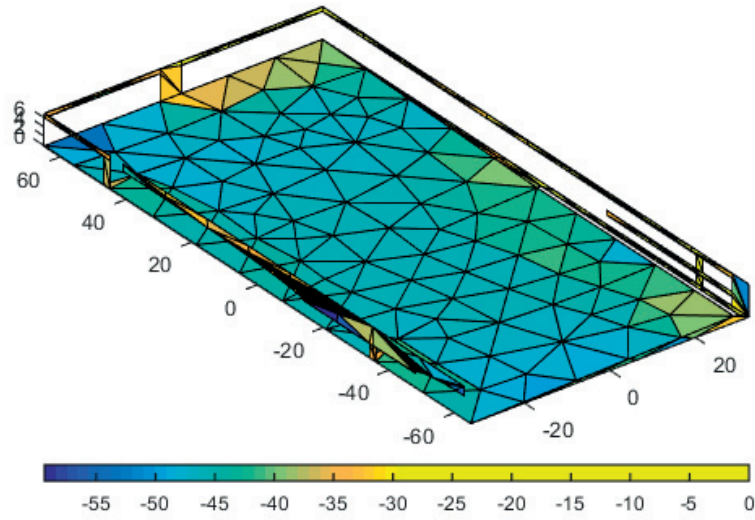
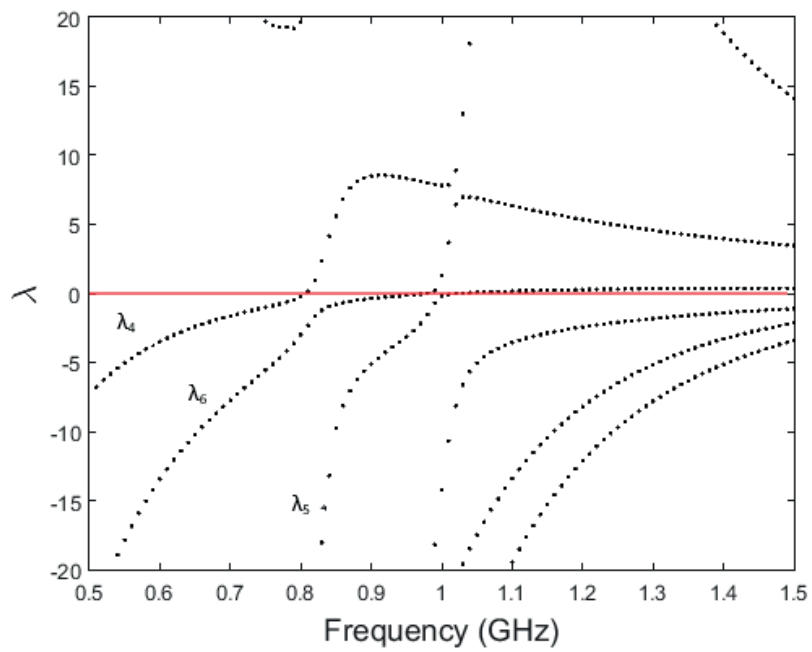Fig. 2.9: Surface eigencurrents of the full structure at 0.97 GHz for mode 5

Fig. 2.10: Eigenmodes of the full structure with T-strip and half-bezel

20

CHAPTER **3**

3 Description of Antennas

3.1 Common Mobile Handset Antennas

An antenna acts as one of the essential components in a mobile phone. It realizes information transmission by converting EM waves into electrical signals or vice versa [21]. A few parameters of mobile handset antenna are important, such as resonant frequency, polarization, impedance, radiation pattern, efficiency, directivity and gain, and Specific Absorption Rate (SAR). The paragraphs below introduce some commonly used mobile handset antennas.

Planar Inverted-F Antenna (PIFA) has been widely used in mobile handsets for many years. It first appeared in the year 1987 [22] with the desirable characteristics of simple construction, high radiation efficiency, low-loss impedance matching and low profile. As presented in Fig. 3.1, Normally, L1 = $\lambda/4$ (λ is the wavelength of the resonant frequency). However, while having so many advantages, one drawback of PIFA is its narrow bandwidth. This drawback is not very important in 2G mobile systems. However when it comes to 4G systems, large bandwidth is required in order for these systems to offer high data rates.
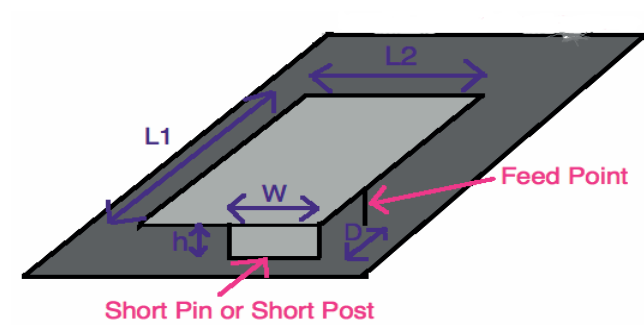

Fig. 3.1: Structure of a PIFA

Whip antenna is a single element antenna which could be taken as one example of monopole antenna. It has been widely used for FM radios, mobile phones' Global Positioning System (GPS) receivers and so on years ago. Basically, whip antenna is flexible, simple to design mechanically and easy to install. The length of the whip is determined by its wavelength, $L = \lambda/4$ (L represents the length of the whip). However, whip antennas may lead to several biological safety issues in specific usage environments. Moreover, the efficiency of whip antennas can be a problem if they are operated with a poor electrical ground system [21].

In this thesis, several kinds of antennas are utilized for the mobile handset, including bezel antenna, IFA antenna, slot antenna and T-strip antenna. More details of these antennas will be provided below.

3.2 Bezel Antenna

Bezel antenna is a relatively new kind of handset antenna, developed in recent years and a commercial application of it can be seen in Fig. 3.2. It is getting more and more widely used in the industry, e.g., "iPhone" and "iWatch". A bezel antenna is equivalent to loop antenna in its operating principle. It can appear in different shapes such as circular, rectangular, triangular and so on. According to its electrical length, it could be classified as an electrically large antenna when $C \approx \lambda$ (C is the circumference of bezel) as well as an electrically small antenna when $C < 0.1\lambda$. Even though electrically small antennas can save a lot of implementation space, the radiation efficiency is quite low, which makes it unlikely to be used in mobile device antenna design. The electrically large loop can resonate when its physical length is an integer multiple of the wavelength.

Fig. 3.2: Industrial design of a bezel antenna for Apple iPhone 4

3.3 IFA Antenna

Inverted-F Antenna (IFA), in general, can be seen as a bent monopole antenna, with an offset feed that facilitates good impedance matching. The whole structure looks like an inverted-F shape and it is mounted on a conducting ground plane.
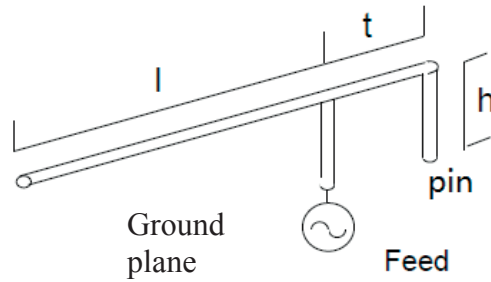

Fig. 3.3: Structure of an IFA

A typical IFA antenna is presented in Fig. 3.3, "h" refers to the height of the IFA. Here, "t" is the horizontal distance between the IFA shorting pin and the IFA feed, whereas "l" represents the length of the IFA's wire segment. The IFA height (h) should be much smaller than the IFA length (l+t). Basically, the whole IFA length determines the resonant frequency of IFA antenna, as given in (5):

$$L = 1 + t \approx \frac{\lambda}{4} \tag{5}$$

3.4 Slot Antenna

In essence, the slot antenna is just a slot through a metal chassis, with the antenna feed connected to each side of the slot. A slot antenna resonates when the slot length L = $\lambda/2$. It has a radiation pattern which is roughly omnidirectional. Slot antennas are widely used in many applications, especially where low-profile or flush mountings are required [23]. The position of the feed affects the efficiency of the slot antenna. Feeding the slot in the middle (as shown in Fig. 3.4) is inefficient. Moving the feed to either side by around $\lambda/4$ leads to better results. As for mobile handset antenna design, slot antenna can be used opportunistically to provide an extra resonance in many antennas such as micro-strip antennas.
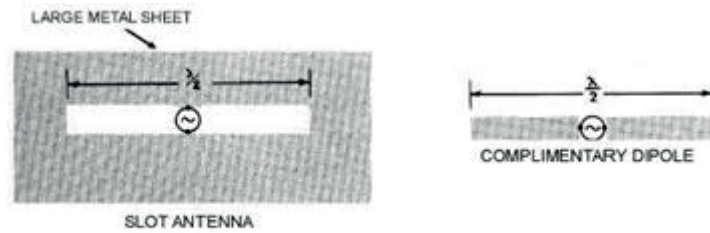
Fig. 3.4: A typical slot antenna [23], shown together with a complementary electric dipole

3.5 T-strip Antenna

In this thesis, T-strip antenna refers to a T-shaped radiating construction loaded along one longer side of the chassis (T-strips along both longer sides are proposed in [20]). As shown in Fig. 3.5, a common T-strip antenna is presented, with either side about the shorting pin having the same length of $L/2$. To meet the needs of multi-band application, the position of the shorting pin can be tuned to make each side having a different length. In this way, The T-strip antenna, when fed off the center, is a dual resonant antenna, with the longer strip resonant at the low frequency band and the shorter strip resonant at the higher frequency band. The T-strip antenna is compact, as well as mechanically and electromagnetically robust, which makes it a good candidate for use in mobile devices.
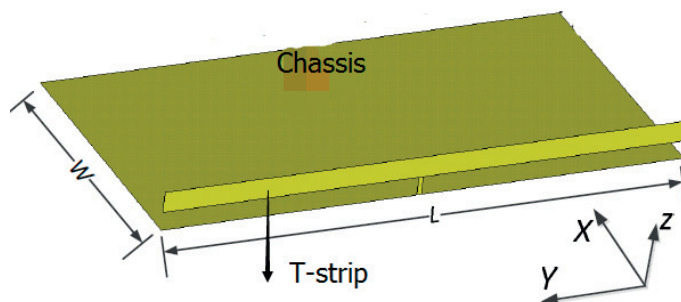

Fig. 3.5: A T-strip structure along the longer side of the chassis (ground plane)

4 Antenna Simulations

4.1 Work Flow

With the TCM analysis done in Section 2.2, the antennas used to excite the modes of interest are now simulated in CST. The dimensions of the whole chassis are 30 mm × 65 mm × 7 mm, as shown in Fig. 4.1. A dielectric substrate with relative permittivity of 2.54, loss tangent of 0.003 and thickness of 0.8 mm is used. In order to save space for other components in a real mobile device (e.g., battery, microphone, speaker, etc.), only the periphery of the chassis is used for antenna design. One part of the periphery is used for the T-strip antenna, whereas the other part is occupied by the reconfigurable antenna, which can be switch between the bezel and IFA modes.
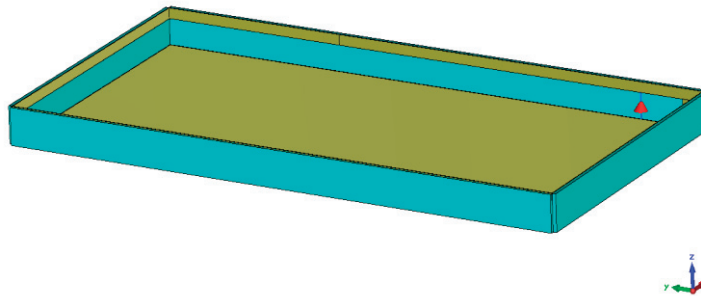

Fig. 4.1: Chassis enveloped in the substrate

The goal of the simulations is to design a dual-band MIMO antenna system with pattern reconfiguration at the low band (below 1 GHz). Moreover, mutual coupling as well as (inter-state and intra-state) correlation parameters should be tuned to be as low as possible. The specifications for the two frequency bands of interest (high and low bands) are presented in Table 1.

TABLE 1: SPECIFICATIONS OF TARGET BANDS

LTE B5 Band	LTE B2 Band
824–894 MHz	1.850–1.990MHz
(824–849 and 869–894)	(1.850–1.910 and 1.930–1.990)
70 MHz Bandwidth	140 MHz Bandwidth

4.2 Full-Bezel Reconfiguration

To simplify the whole design at the beginning, the first trial was to make a single reconfigurable antenna. In order to make the reconfigurable antenna to work in both IFA and bezel states, two PIN diodes were included for controlling the antenna to work in either the IFA mode or the bezel mode.

As shown in Fig. 4.2, when "diode 1" is off and "diode 2" is on, the IFA mode is created. Since the other side is not connected to any feed directly, the part "Wing1+Meander line+Wing2" can simply be ignored as it has little influence on the antenna performance. As a result, the antenna could be simplified as shown is Fig. 4.3. On the other hand, when "diode 1" is on and "diode 2" is off, the pin connects the gap between "Wing1" and "IFA wing". This turns the structure into a bezel antenna, as shown is Fig. 4.4. In this case, the influence of the "IFA wing" can be ignored.

In the simulation, a shorting wire or an opening is used to represent the on or off state of the PIN diode for simplification. As it is known, in reality, there exists a small resistance or a high capacitance for the on or off state. As a result, the bandwidth can be larger whereas the radiation efficiency can be lower in real implementation compared to the simulated results using simplified diodes. To distinguish the two antennas, the reconfigurable antenna will be called to be operating in "IFA state" or "bezel state".
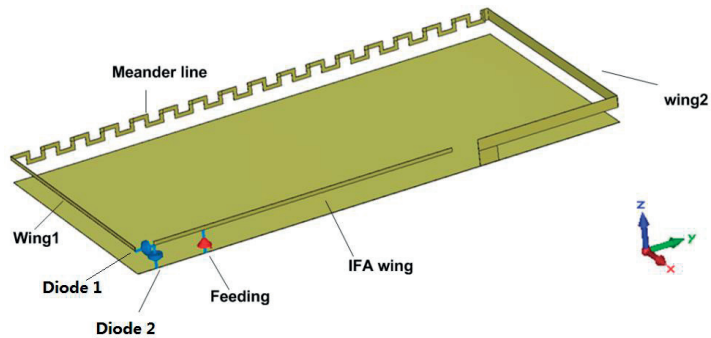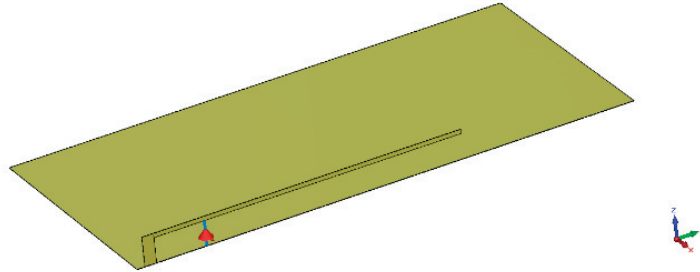

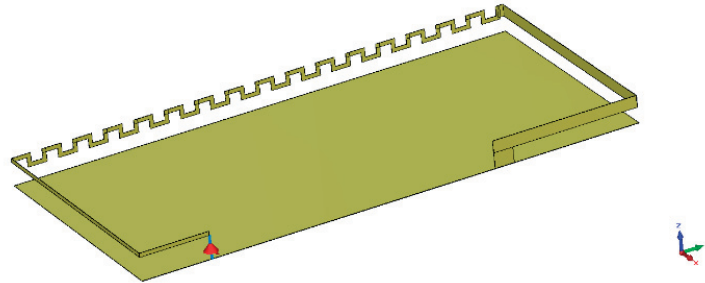Fig. 4.2: IFA/bezel reconfigurable antenna design

26

Fig. 4.3: IFA state

Fig. 4.4: Bezel state.

Theoretically, the lengths of the IFA and bezel antenna should be set according to (6) and (7):

$$L_{IFA} = \lambda/4 \tag{6}$$

$$L_{bezel} = \lambda \tag{7}$$

Basically, the resonant frequencies are reversely proportional to the lengths of these antennas. Accordingly, for the IFA state, the length of "IFA wing" determines the resonant frequency, which is easy to tune. However, it is tougher to tune the bezel state as L_{bezel} consists of L_{Wing1}, $L_{Meander\ line}$ and L_{Wing2} (i.e., respective lengths of the "Wing1", "Meander line" and "Wing2" sections). Efforts were made to make L_{bezel} to be one wavelength for the desired resonant frequency (around 860 MHz). However, since the size of chassis is limited, there is no luxury of space for the theoretical length of around 300 mm. This is the reason for the initial straight long wire in the "Meander line" section (not shown here) was meandered (as shown in Fig. 4.2) to increase the electrical length.

27

The reflection coefficients of the antenna in the two states are shown as in Fig. 4.5. According to the 6 dB bandwidth criterion for mobile handset antennas, the bezel state has a bandwidth of 100 MHz, ranging from 780 MHz to 880 MHz, whereas the IFA state has a bandwidth of 70 MHz, ranging from 820 MHz to 890 MHz. The bandwidth of the IFA state is partly attributed to the radiation of the fundamental chassis mode.
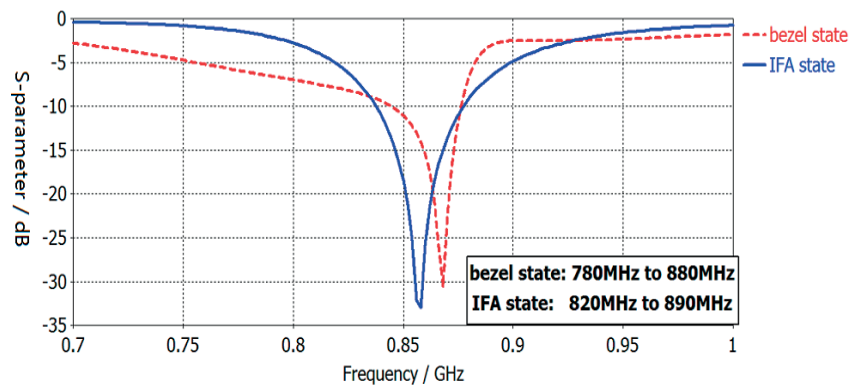

Fig. 4.5: Reflection coefficients of the IFA/bezel reconfigurable antenna

In Fig. 4.6, it can be seen that for the IFA state, the currents flow from the antenna feed to the whole IFA antenna as well as the part of the ground chassis below the IFA antenna. For the bezel state, it is observed in Fig. 4.7 that the currents flow from the feed to the entire bezel (along all four sides).
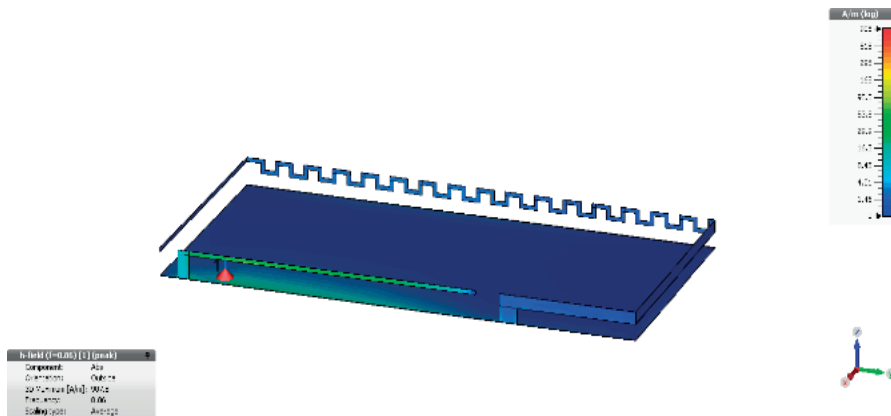

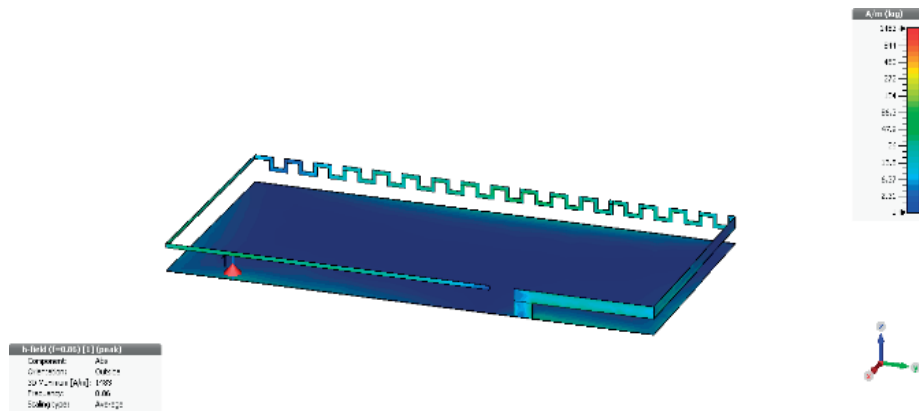Fig. 4.6: IFA state current distribution at 870 MHz

Fig. 4.7: Bezel state current distribution at 870 MHz

The radiation patterns of both states at 870 MHz are shown in Figs. 4.8 and 4.9. As shown in Fig. 4.8, the antenna working in the IFA state has a radiation pattern that is almost omnidirectional in the x-z plane, and it has two coaxial nulls along the y-axis (i.e. similar to the pattern of an electric dipole oriented along the y-axis). It can be seen in Fig. 4.9 that the antenna working in the bezel state has a radiation pattern with higher gains in the –z and +z directions, with more power radiated to the –z direction.

According to the CST simulation data, the total efficiency of the IFA state is 0.944, and that of the bezel state is 0.934. Moreover, according to the simulation results as well as some calculations, the inter-state ECC of 0.073 is achieved.
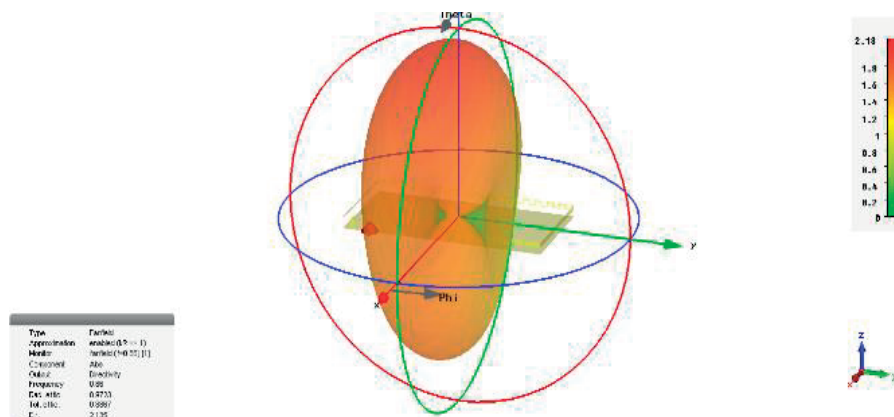

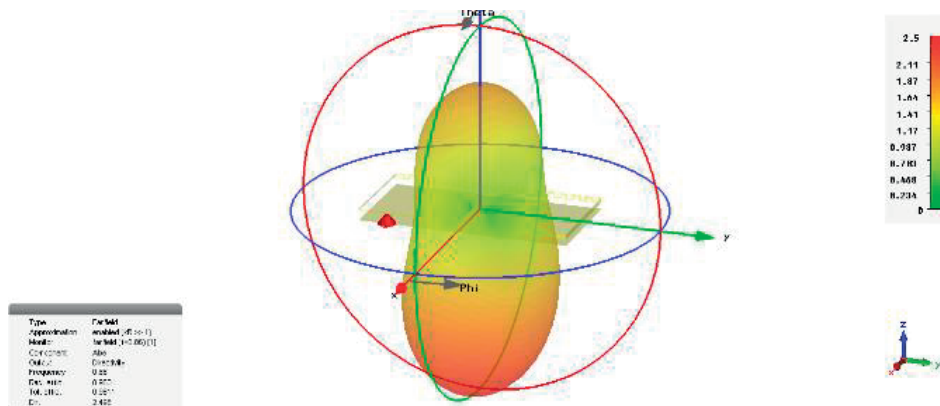Fig. 4.8: IFA state radiation pattern at 870MHz

Fig. 4.9: Bezel State Radiation Pattern at 870MHz

To sum up, the first design of the single reconfigurable antenna works relative well in the low band frequency. Both states have good bandwidth performance and the inter-state correlation is very low.

4.3 Half-Bezel Reconfiguration

For the full-bezel loaded chassis in the previous section, only one antenna can be situated along the periphery. Considering that MIMO application needs a second antenna along the periphery, the reconfigurable antenna structure must be compressed, and at least one long edge should be saved for the second antenna.

As mentioned in Section 2.2, the length of the bezel antenna can be reduced by half through connecting it with the ground plane, i.e., taking advantage of the ground plane to complete a full wavelength bezel. Moreover, different from the structure in Section 4.2, the IFA wing is used as part of the bezel antenna. Finally, two edges are saved for MIMO application as shown in Fig. 4.10.
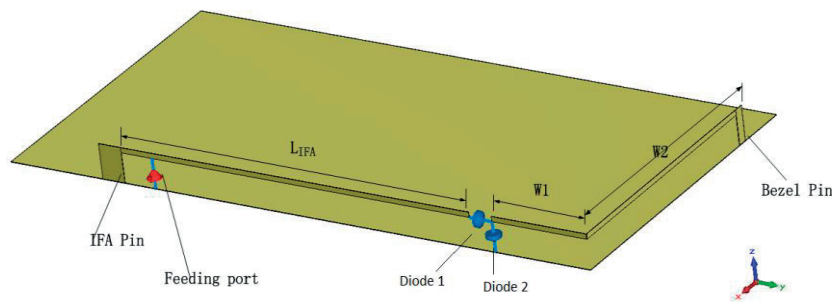

Fig. 4.10: Compressed IFA/bezel Reconfigurable Antenna Single Band Design

30

In this case, while "diode 1" is off and "diode 2" is on, the whole structure works in the IFA state. Resonance frequency is mostly determined by L_{IFA}. While "diode 1" is on and "diode 2" is off the antenna turns to the bezel state, the length of "L_{IFA}+W1+W2" determines the bezel antenna resonance frequency.

The reflection coefficients of the antenna in the two states are shown in Fig. 4.11. According to the 6 dB bandwidth criterion for mobile handset antennas, the bezel state has a bandwidth of 20 MHz, ranging from 870 MHz to 890 MHz, whereas the IFA state has a bandwidth of 60 MHz, ranging from 840 MHz to 900 MHz.
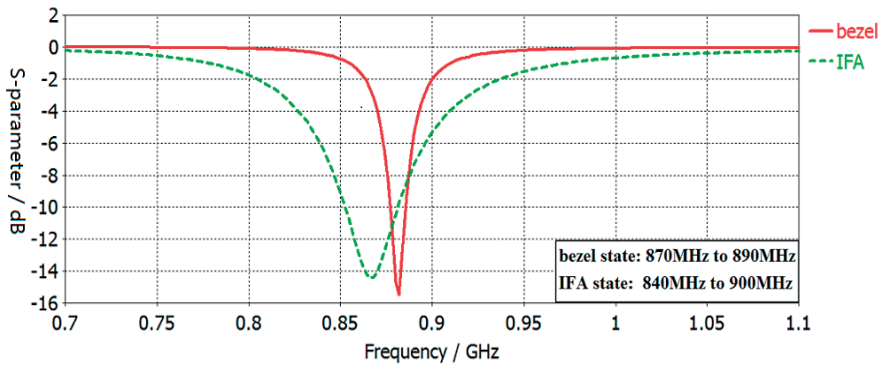

Fig. 4.11: Compressed IFA/bezel reconfigurable antenna single-band reflection coefficients

Compared to full-bezel in Section 4.2, the bandwidth performance for the bezel state is much worse. According the TCM analysis of this structure, a really steep slope is found for the bezel state, which means the bandwidth is theoretically narrow. Generally speaking, in order to have more space saved for MIMO application, the bandwidth in the bezel state could not avoid being sacrificed.

The current distributions of both states are presented in Figs. 4.12 and 4.13. In Fig. 4.12, currents can be seen flowing in the IFA antenna only, and no currents flow over the other strip. In Fig. 4.13, the currents flow from the feed point to the whole half-bezel antenna and the chassis below.
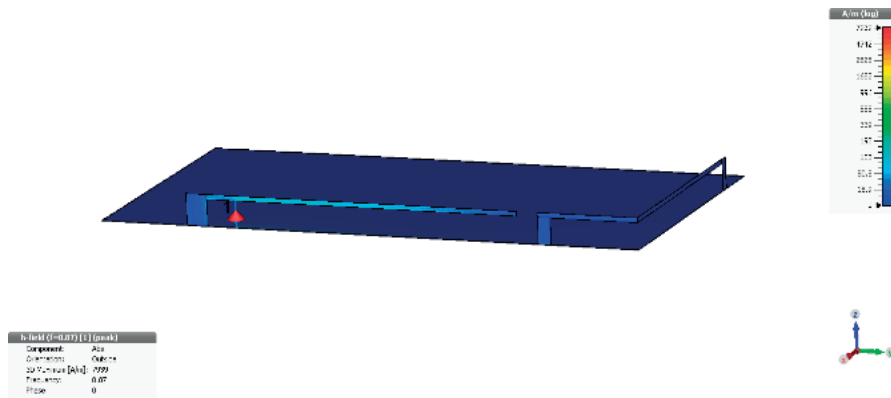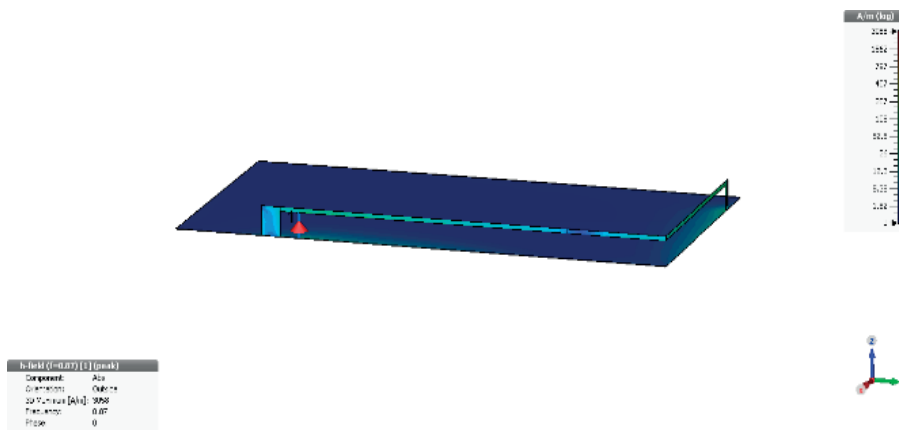
Fig. 4.12: IFA state current distribution

Fig. 4.13: Bezel state current distribution

For the radiation pattern, there is not too much difference compared with the full-bezel antenna, as can be seen in Figs. 4.14 and 4.15. The "inter-state" ECC is 0.23 at the frequency of 870 MHz.

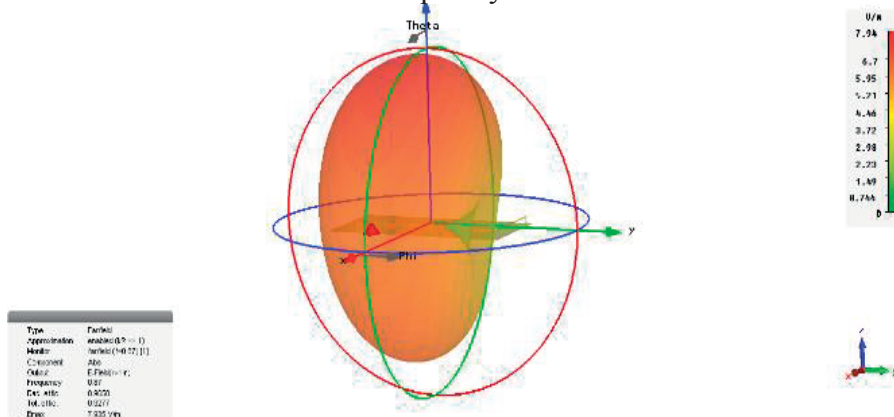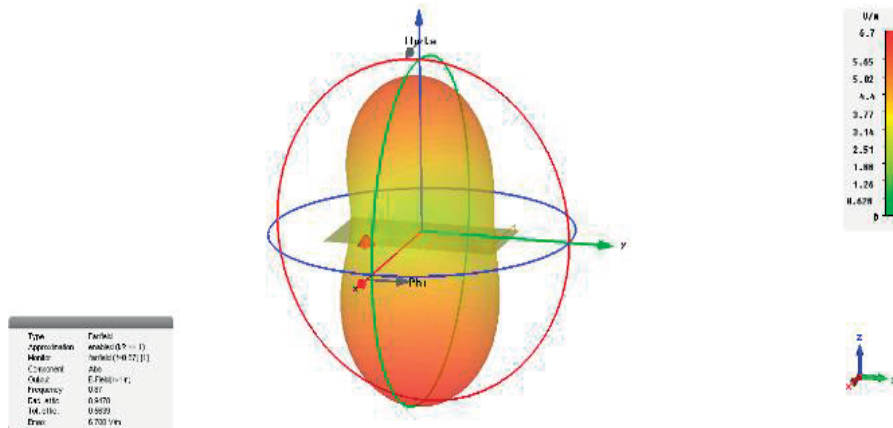Fig. 4.14: IFA state radiation pattern

Fig. 4.15: Bezel state radiation pattern

4.4 Dual-Band Realization for IFA/bezel Antenna

In order to achieve dual-band operation, a shorter strip is added below the original IFA antenna, sharing the same feeding port and same pin, as shown in Fig. 4.16. The length of the extra wing L_{IFA2} determines resonant frequency of the high band. According to theoretical result as well as the adjustment from some simulations, the length of the shorter strip is set as $L_{IFA2} = 37$ mm to obtain the resonant frequency of around 1950 MHz.

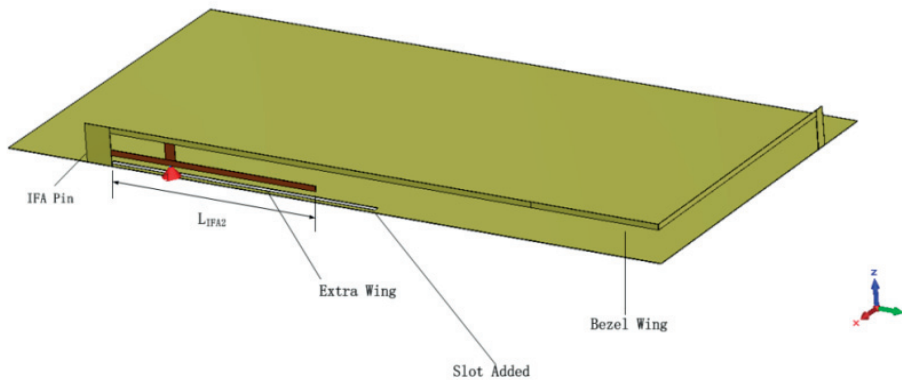Fig. 4.16: Extra wing added in the bezel state for dual-band resonances

Moreover, as shown in the Fig. 14.6, there is a slot added on the chassis. The first intention of having the slot is to get some resonance here at the high frequency according to [24].

Even though this slot is not an exactly a "slot antenna", some current will flow by so as to resonate at the high band. However, this step does not work

well in this case, since even though there is some resonance from the desired frequency, it is too weak to make a real difference. In the final design, the slot is still kept, but with some optimization of the length and width. The reason to keep the slot is not for an extra resonance, but to change the current distribution so that better bandwidth will be achieved in the high band. A little refinement is set according to simulation results and finally the best result with "slot" length of 60 mm is kept.
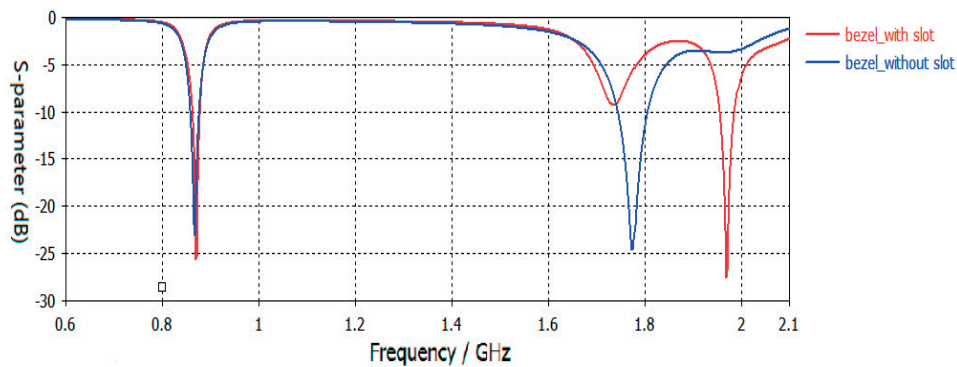

Fig. 4.17: Reflection coefficients for the bezel state with/without slot
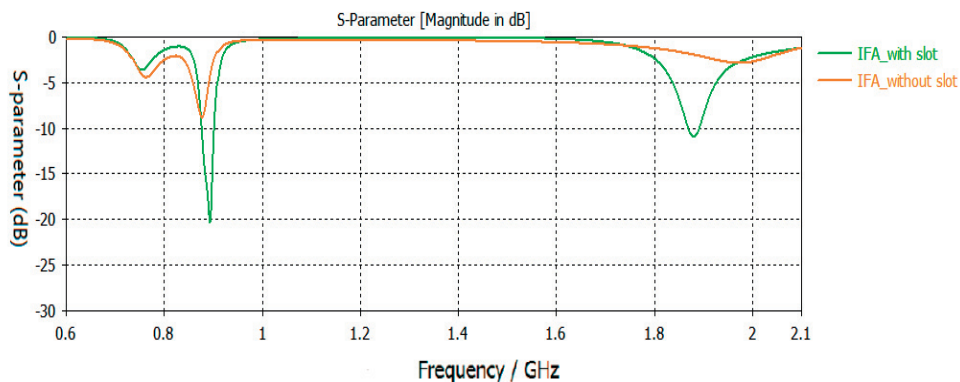
Fig. 4.18: Reflection coefficients for the IFA state with/without slot

Results in Figs. 4.17 and 4.18 show the simulated reflection coefficient (S_{11}) results for the bezel state with/without slot. For the bezel state, in the low band, not too much difference is introduced by the slot, whereas in high band, the resonant frequency shifted from 1.95 GHz to 1.75 GHz, which merges with the other resonant frequency at around 1.7 GHz. In the IFA state, the slot improved the performance a lot. The matching is much better with the slot so that more bandwidth is gained in the low band. More importantly, without the slot, the IFA state cannot resonate well in the high band.

Fig. 4.19: S11 Results of Bezel/IFA State in High Band

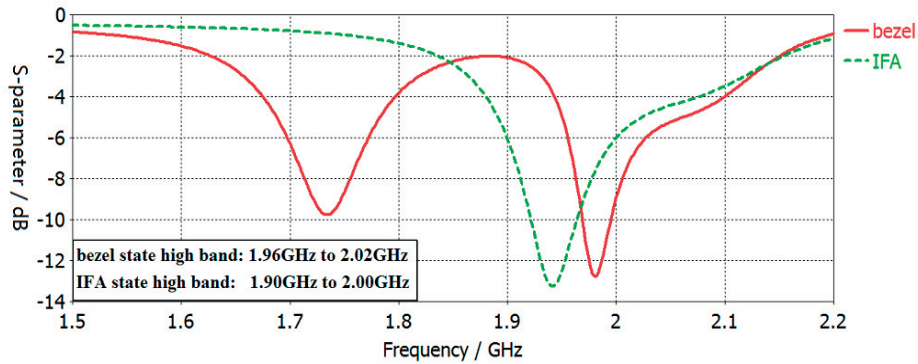The reflection coefficients for the two states (with the slot) at the high-frequency band are shown in Fig. 4.19. The low-frequency band is not influenced by the extra short strip and not shown here for clarity of figure. It is observed that in the bezel state, there is one more resonance at around 1.73 GHz. This is not from the "slot" or the "shorter strip" added, but it is actually introduced from higher-order modes of the bezel antenna.

4.5 T-strip Antenna Design

The T-strip antenna is chosen to be the second antenna for MIMO application, due to it introducing a third CM at frequencies below 1 GHz.

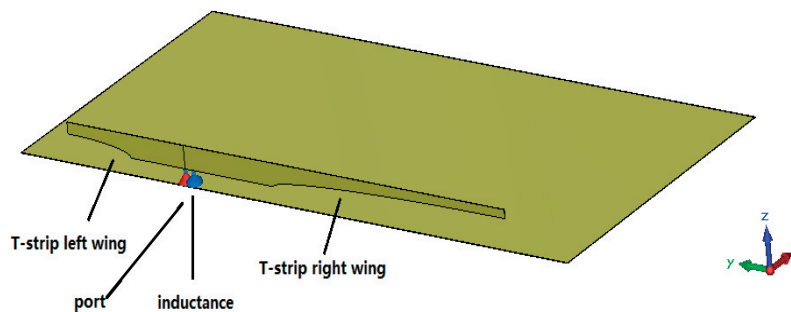Fig. 4.20: T-strip antenna structure

To work in dual-band, the T-strip antenna in Fig. 3.5, based on [20] is modified, as presented in Fig. 4.20 (the version with two T-strips proposed in [16]). A parallel inductor of 1 nH is put between the T-strip and the ground plane. The length of the T-strip left wing and right wing is set to be 28 mm and 76 mm respectively. In addition, curves are cut in both wings

35

which lead to better impedance matching [16]. This design afforded around 4 MHz more bandwidth and 30 MHz shift to the right in the low band, as well as 18 MHz more bandwidth and 70 MHz shift to the right in the high band. The reflection coefficients for both the low- and high-frequency bands are shown in Fig. 4.21. A bandwidth of around 50 MHz is achieved in the low band and 220 MHz in the high band.
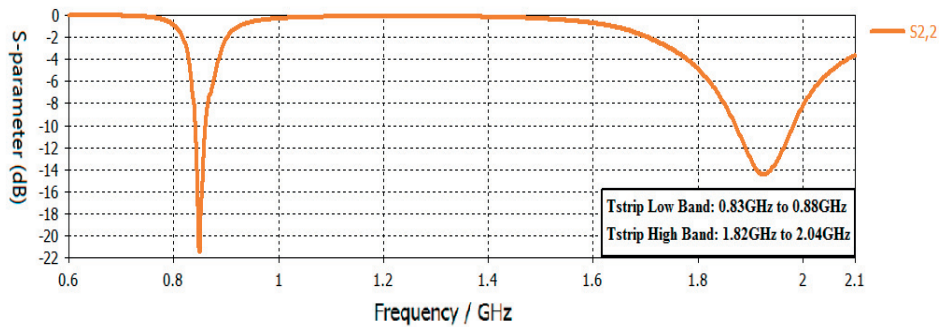
Fig. 4.21: Reflection coefficient of the T-strip antenna

Current distributions of the T-strip antenna are shown in Figs. 4.22 and 4.23 for the low- and high-frequency bands, respectively. It is quite obvious that in the low band, the currents go over the right wing and the ground plane part just beneath the right wing. In the high band, however, the currents go over the left wing and the ground plane part just under it.

The radiation patterns for this antenna are shown in Figs. 4.24 and 4.25 for low- and high-frequency bands, respectively. In the low band, the radiation pattern is almost omnidirectional in x-z plane, while there are two nonobvious coaxial nulls in the direction of the y-axis. Less power radiates in the +x direction due to the non-symmetric structure.

Fig. 4.22: T-strip antenna current distribution in the low band

Fig. 4.23: T-strip antenna current distribution in the high band
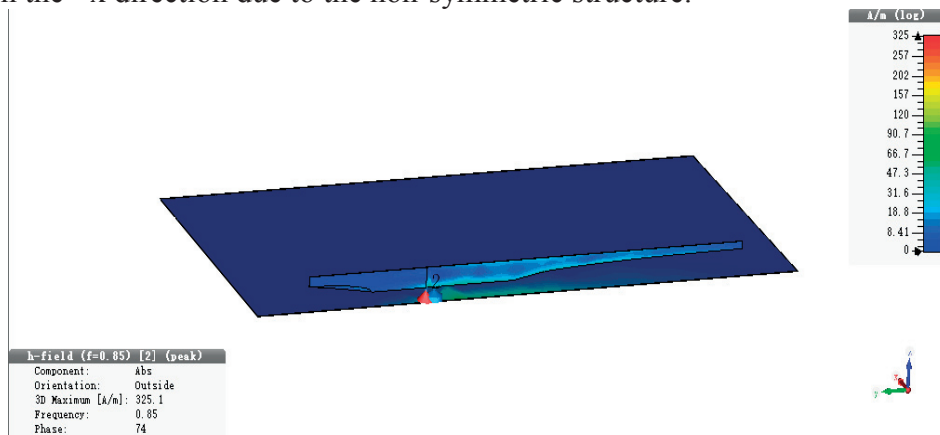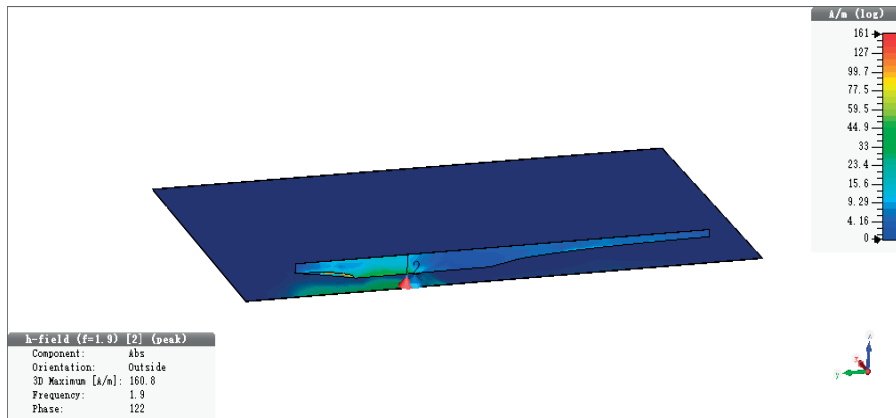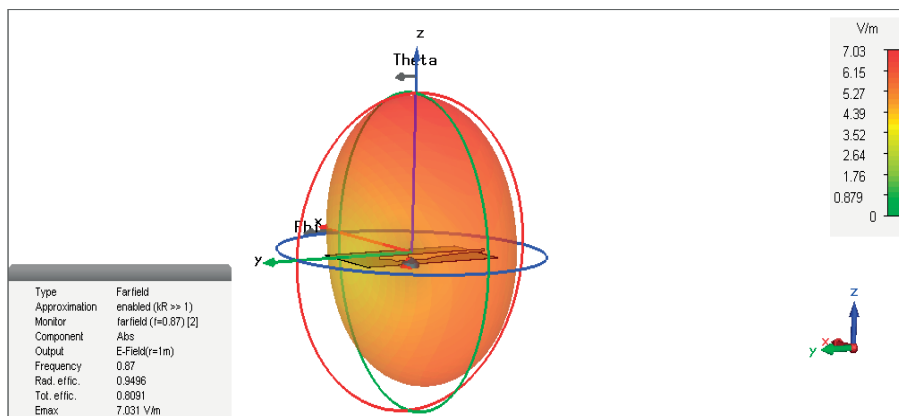

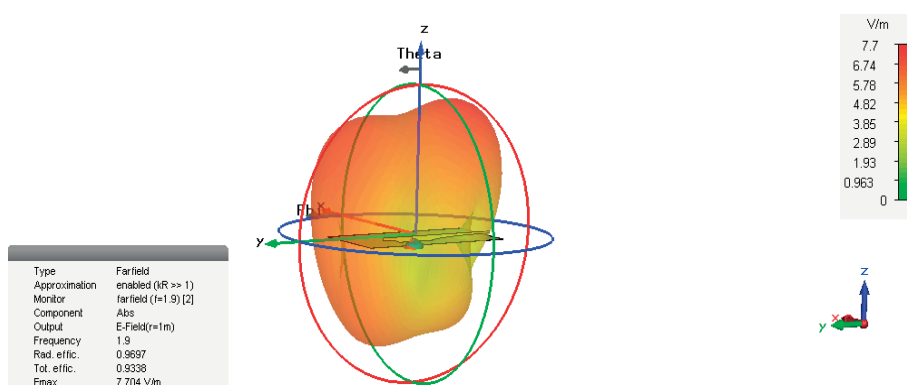Fig. 4.24: T-strip antenna radiation pattern in the low band

Fig. 4.25: T-strip antenna radiation pattern in the high band

37

5 Results and Discussions

By combining the T-strip antenna and the IFA/bezel reconfigurable antennas mentioned in Chapter 4, the final structure is more or less fixed. Nevertheless, to achieve a good design, more detailed modifications are needed, as the inter-state and intra-state correlations as well as the mutual coupling should be taken into consideration simultaneously. In this chapter, the focus is more on the performance at the low band, since it is much more challenging due to the limited area available on the terminal chassis.

*5.*1 Trade-Off in Low-Band Mutual Coupling of Two States

When the antennas are implemented for MIMO application, it is found that in the bezel state the coupling coefficient S_{12} = -8 dB, whereas S_{12} = -5dB in the IFA state. This implies very high mutual coupling especially for the IFA state, as over 30% of the radiating energy is coupled to the other antenna when one antenna is radiating. The method for decoupling and achieving a trade-off in performance is described below.

Generally, it was found that only decoupling methods involving small alterations to the structure could be used to improve mutual coupling performance to avoid significant impacts on other performance parameters.

5.1.1 Mutual Coupling Improvement for IFA State

After analyzing the current distributions from the antenna simulations of the IFA state, strong currents are found to flow across the edges from one port to the other port. One idea of improving the coupling performance is to reverse the T-strip antenna in the x-z plane, as shown in Fig. 5.1. Prior to the change, the modes excited by the IFA antenna and the T-strip antenna are non-orthogonal. With this modification, the two antennas can excite orthogonal modes. As a result, currents from one antenna no longer couple to the other antenna.

After this modification, the coupling coefficient S_{12} of -15dB is achieved in the IFA state, which is significantly better than the earlier result of -5dB. However, with this structural change, mutual coupling becomes much higher for the bezel state (with S_{12} = -4 dB). More modifications are needed to optimize the coupling in the bezel state. In addition, the mutual coupling at the high-frequency band also increases slightly, though still negligible.
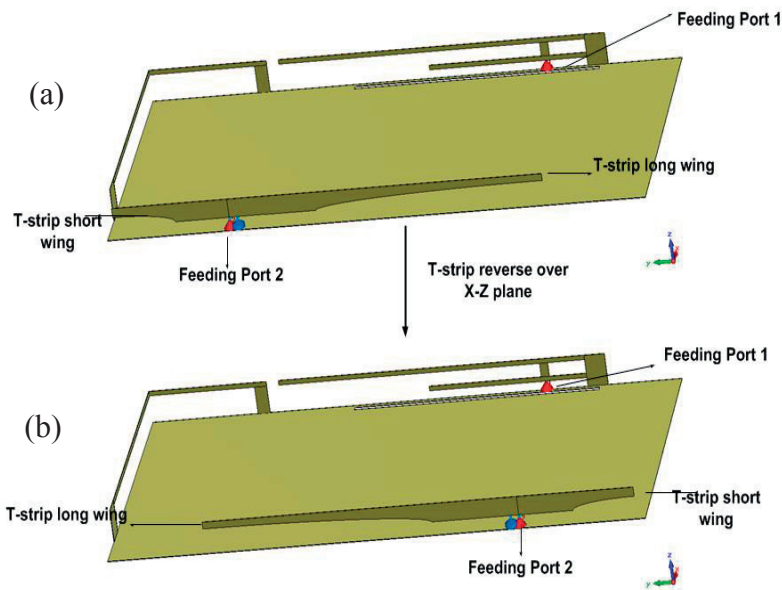
Fig. 5.1: Dual-band MIMO antenna with (a) T-strip antenna and (b) T-strip antenna reversed

5.1.2 Mutual Coupling Improvement for Bezel State

In order to further reduce the mutual coupling in the bezel state, several strategies can be adopted. A commonly used one is called "Defected Ground Structure" (DGS) [14], which basically means cutting some slots on the chassis or even just cutting the whole structure into two parts. However, this is unacceptable for the antenna in this thesis, since it may affect the performance of other electronic devices in a real handset. Thus it is not recommended for mobile antenna design.

Another way of decoupling is called "connecting line" [25] which basically uses a line to connect antennas. The mutual coupling can be reduced by self-cancellation of the induced common ground as well as the near-field currents. Efforts were made in adding some "connecting lines" for this case. However, all of those trials fail to yield satisfactory overall results, since other performance parameters of the antenna (such as resonant frequency,

bandwidth and intra-state correlation) are degraded by the connecting line when the mutual coupling is reduced.

One successful trial in this case is to add an extra wing and pin as shown in Fig. 5.2. With this modification, some currents are directed to the added wing. In addition, the position of port 1 is optimized, moving it as far as possible from the other port (as shown in the bottom figure in Fig. 5.2).

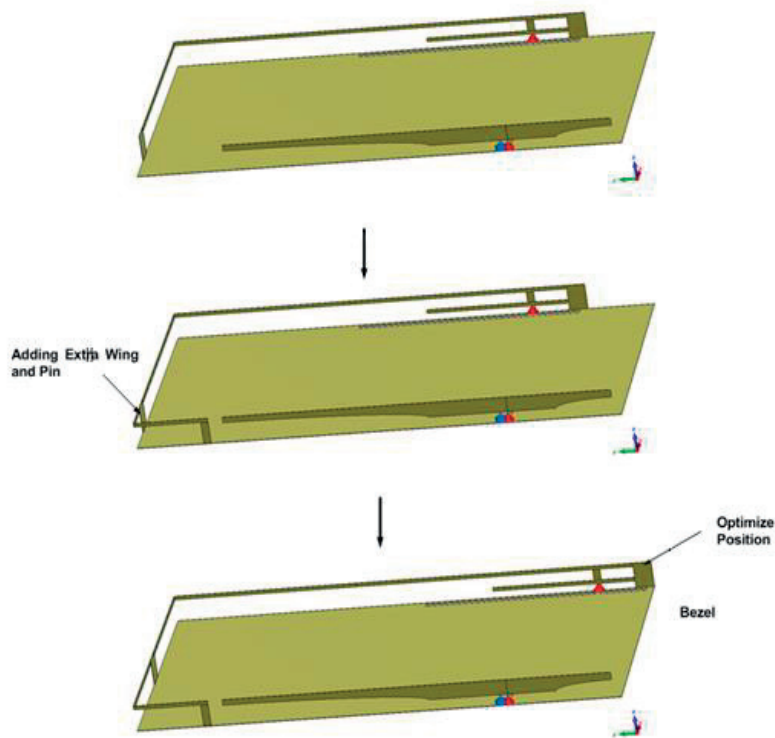

Fig. 5.2: Bezel State Mutual Coupling Modification

After the final optimization, the mutual coupling result of S_{12} = -7dB is achieved for the bezel state (improved from -4dB). As a trade-off, the mutual coupling of S_{12} = -10dB is obtained for the IFA state (degraded from -15dB). Moreover, another trade-off is that, the inter-state correlation becomes higher, i.e., from 0.14 to 0.3.

5.2 Final Structure and Simulation Results

The final structure is shown in Fig. 5.3. Parameters are set to be $L_{slot} = 60$ mm, $L_{IFA2} = 38.5$ mm, $L_{IFA} = 75$ mm, $W_0 = 47$ mm, $W_1 = 33$ mm, $W_2 = 27$ mm, $W_3 = 20$ mm, $L_{T\text{-}Long} = 76$ mm, $L_{T\text{-}Short} = 28$ mm. Moreover, the inductor has a value of 1 nF.
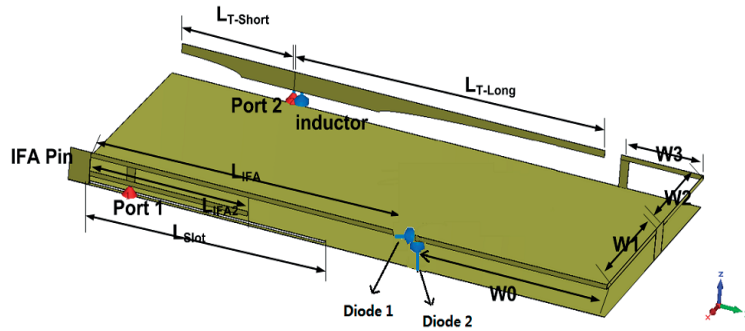
Fig. 5.3: Final structure of the MIMO antenna with reconfigurable IFA/bezel state

5.2.1 Scattering parameters

The scattering parameters (S parameters) of the final structure are shown in Figs. 5.4 and 5.5. Here it can be seen that the bandwidth of the bezel antenna (i.e. in the bezel state) is relatively narrow, i.e., 20 MHz in the low frequency band and 50 MHz in the high frequency band. In the bezel state, the T-strip antenna has a bandwidth of 60 MHz in the low band and 110 MHz in the high band. Mutual coupling is -7 dB and -9 dB for the low and high bands. In the IFA state, the IFA antenna bandwidth is 60 MHz in the low band and 80 MHz in the high band, whereas the T-strip antenna has a bandwidth of 60 MHz in the low band and 110 MHz in the high band. The coupling is -10 dB and -8 dB in the low band and high band, respectively.

Fig. 5.4: S parameters of the final structure in the IFA state
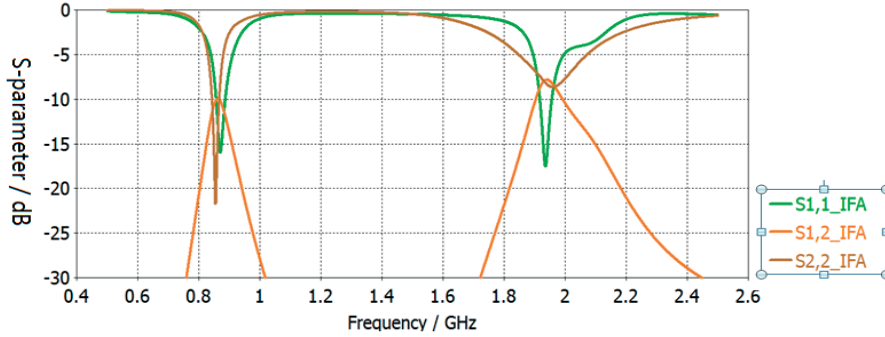
Fig. 5.5: S parameters of the final structure in the bezel state

5.2.2 Envelope Correlation Coefficient

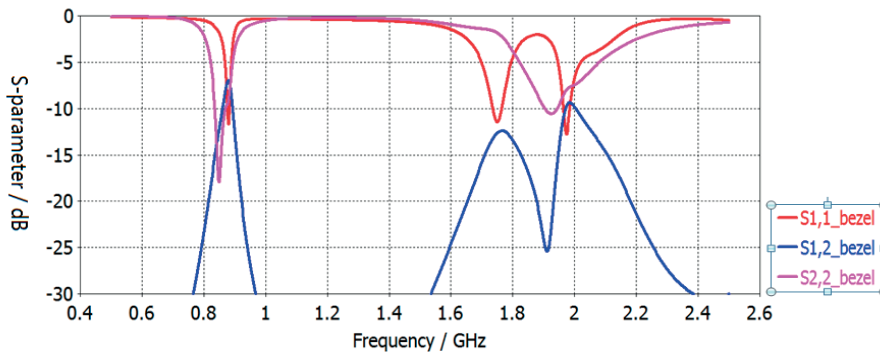The "intra-state correlation" (i.e., correlation of the MIMO antenna in a given state) was calculated with a post-processing feature in CST, and the results are shown in Fig. 5.6. Generally, the ECC is below 0.2 in the desired frequency bands, which is a satisfactory result. The "inter-state correlation" was calculated using Matlab codes with the radiation pattern information obtained from CST. The "inter-state (envelope) correlation" is 0.3 at the center frequency of the low-frequency band, which is not a very low value. However, as discussed before, a trade-off is made here to achieve a smaller mutual coupling in the bezel state. One thing to note is that, since in this thesis only reconfiguration in the low band frequency is realized, the "inter-state correlation" is expected to be high in the high band (close to 1.0), as the two states are sharing the same radiating structure in the high band.

Fig. 5.6: Intra-state Correlation for each State

5.3 Eigenmode Radiation Pattern and Final Radiation Pattern

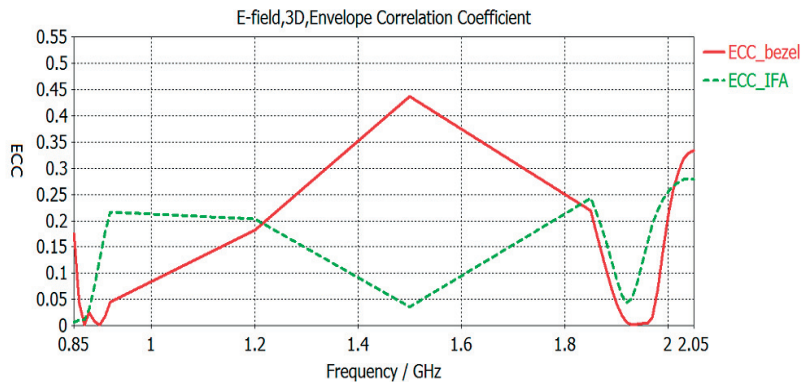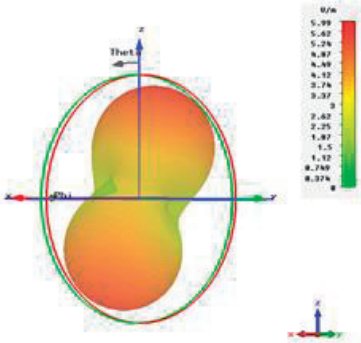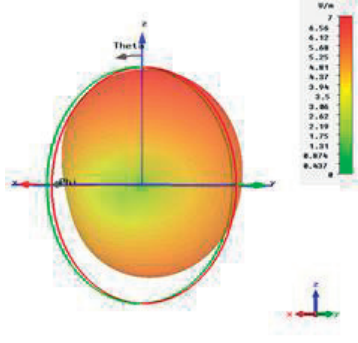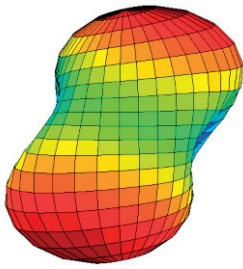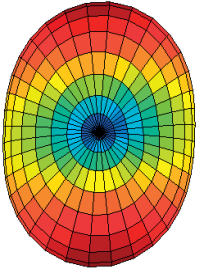At this point, the final design is taken for further investigation with regard to the far fields. The far field results from CST are compared with the far field results given by a TCM analysis in Matlab, in order to analyze which modes are actually excited by the antennas.

The procedure of obtaining the theoretical results is as follows:
- The structure model is exported from CST and meshed.
- The meshed model is imported into Matlab and matrices with geometric data are produced.
- The impedance matrix is calculated using the Method of Moments (MOM), which enables us to perform further calculations for:
  - Eigenvalues of CMs over a frequency range.
  - Far-field pattern and surface currents of the each CM.

In Table 2, the radiation patterns from CST are presented in the first row, whereas those from TCM analysis are shown in the second row. Even though the scaling of the plots from the TCM analysis is qualitative whereas the CST gives exact numbers based on the exact parameters of the simulation, it is still clear that the radiation patterns of the antennas greatly follows the CM patterns of the structure. Therefore, it is proven that the desired CMs are successfully excited.

TABLE 2: RADIATION PATTERN COMPARISON FOR BEZEL STATE
CONFIGURATION AT 1 GHZ

Bezel State		
	Bezel	T-Strip
CST Result		
CM results		

Similarly, in Table 3 the radiation pattern results for the IFA configuration are presented. Again both methods yield similar results which is a verification that specific eigenmodes (or CM), with their corresponding eigenvalues and characteristic current distributions, have been selectively and successfully excited by the configuration of antennas designed.

It is noted that the theoretical results for each eigenmode is produced for the resonant frequency of that mode (i.e., eigenvalue equals to zero for that frequency). This along with the fact that CST uses different meshing technique and meshing density than the imported model to Matlab can cause some deviations which lead to differences between the two results. Nevertheless, overall the results presented by both methods are in good agreement.

44

TABLE 3: RADIATION PATTERN COMPARISON FOR THE IFA STATE
CONFIGURATION AT 1GHZ

IFA State		
	IFA	T-Strip
CST Result		
CM results		

CHAPTER **6**

6 Conclusions

In this thesis, the main focus is on designing a dual-band pattern reconfigurable MIMO antenna using TCM analysis and full-wave antenna simulations. Low correlation and low mutual coupling between the reconfigurable states and the MIMO antennas were achieved.

First, the background of TCM was studied, and the CMs of the simple ground plane with the dimension of 130 mm × 65 mm × 7 mm were simulated. After that, to create more orthogonal modes at frequencies below 1 GHz, modifications on the chassis were made, and their CMs were also investigated. Based on [15], and [24], bezel mode as well as T-strip mode is proposed for MIMO application. Moreover, with suitable modifications of the bezel mode, the IFA mode is achieved for reconfigurability. All these three modes (bezel, T-strip and IFA) are orthogonal to one another.

As the next step, high frequency TCM analysis provided methods such as adding an extra IFA wing and creating a slot antenna in the original structure to support multiband operation at a higher band. Adjustments were made so that better bandwidth performance of each state could be achieved.

Finally, trade-offs between mutual coupling and envelope correlation coefficient (ECC) were made to achieve better MIMO antenna performance. Modifications made for decreasing mutual coupling were carried out by modifying the T-strip mode and introducing a "connecting line". After obtaining the final structure in Fig. 5.3, the radiation patterns of different modes as excited by the corresponding antenna feeds were compared with the theoretical ones to verify the final results. Good agreement was found, indicating that the desired modes were successfully excited by the dual-band reconfigurable MIMO antenna.

CHAPTER 7

7 Future Work

Firstly, the work presented in this thesis is based on theoretical results as well as simulations in both Matlab and CST. Therefore, one possible topic for future work is the fabrication of the final antenna structure for experimental verification. The simpler approach is to implement two MIMO antennas, one for the bezel state and another for the IFA state. Alternatively, real PIN diodes can be included to allow for full reconfiguration of the two states using one single MIMO antenna prototype. However, this may require the properties of the PIN diodes to be incorporated into the simulations, to achieve more accurate simulation results (for fine-tuning purposes) prior to prototype fabrication.

Moreover, when the actual reconfigurable MIMO antenna prototype is built, tests could be performed in real propagation channels to determine the degree to which the pattern reconfigurable MIMO antennas can improve the overall communication performance. This is a topic of interest as there are still some discussions on whether reconfigurable antennas are useful to supplement the effectiveness of conventional (fixed) MIMO antennas in improving communication performance.

Additionally, other aspects of similar antennas can be investigated. As there is a trend in using mobile handsets of bigger form factors, TCM-based antenna design is expected to be of more importance. The bigger the chassis become, the more space can potentially be used for designing antennas for MIMO purposes. For LTE-Advanced and beyond systems, four or more MIMO-capable antennas are needed on the same chassis and reconfigurability is also expected to play an important role by further improving the effectiveness of the MIMO antennas.

References

[1]. Elfergani I.T.E., Abd-Alhameed R.A., See C.H, Sadeghpour T., Dama Y., Jones S.M.R., Excel P.S., "A compact size reconfigurable PIFA antenna for use in mobile handset", XXXth URSI General Assembly and Scientific Symposium (GASS), 2011, pages 1-4.

[2]. Lee S.W., Sung Y., Park J.Y., Lee S.J, Hur B.J., "Frequency reconfigurable antenna using a PIN diode for a mobile handset application", 7th European Conference on Antennas and Propagation (EuCAP), 2013, pages 2053-2054.

[3]. Elfergani I.T.E., Abd-Alhameed R.A., See C.H, Sadeghpour T., Jones S.M.R., "Reconfigurable antenna design approach for mobile applications and a technique for harmonics suppression", Loughborough Antennas and Propagation Conference (LAPC), 2011, pages 1-4.

[4]. Kumar K.K., Hum S.V., "A pattern reconfigurable chassis-mode MIMO antenna", IEEE Transactions on Antennas and Propagation, volume: 62, 2014, pages 3290-3298.

[5] Kishor K.K., Hum S.V., "A reconfigurable chassis-mode MIMO antenna", 7th European Conference on Antennas and Propagation (EuCAP), 2013, pages 1992-1996.

[6]. Garbacz, R.J., Turpin, R., "A generalized expansion for radiated and scattered fields", IEEE Transactions on Antennas and Propagation, volume: 19, 1971, pages 348-358.

[7]. Harrington R.F., Mautz J.R., "Theory of Characteristic Modes for conducting bodies", IEEE Transactions on Antennas and Propagation, volume:19, 1971, pages 622-628.

[8] Harrington R.F., Mautz J., Chang Y., "Characteristic modes for dielectric and magnetic bodies", IEEE Transactions on Antennas and Propagation, volume:20, 1972, pages 194-198.

[9] Garbacz R.J., Pozar D.M., "Antenna shape synthesis using characteristic modes", IEEE Transactions Antennas and Propagation, volume:30, 1982, pages 340-350.

[10] Cabedo-Fabres M., Antonino-Daviu E., Valero-Nogueira A., Ferrando-Bataller M. "The Theory of Characteristic Modes revisited: A contribution to the design of antennas for modern applications", IEEE Antennas and Propagation Magazine, 2007, pages 52-68.

[11] Antonino-Daviu E., Cabedo-Fabres M., Gallo M., Ferrando-Bataller M., Bozzetti M., "Design of a multimode MIMO antenna using characteristic modes", 3rd European Conference on Antennas and Propagation (EuCAP), 2009, pages 1840-1844.

[12] Miskovsky P., von Arbin A., "Evaluation of MIMO handset antennas with decorative metal elements, using characteristic modes", IEEE Antennas and Propagation Society International Symposium (APS), 2014, pages 1423-1424.

[13] Krewski A., Schroeder W.L., Solbach K., "Multi-band 2-port MIMO LTE antenna design for laptops using characteristic modes", Loughborough Antennas and Propagation Conference (LAPC), 2012, pages 1-4.

[14] Manteuffel D., Martens R., "A concept for MIMO antennas on small terminals based on characteristic modes", International Workshop on Antenna Technology (iWAT), 2011, pages 17-20.

[15] Miers Z., Li H., Lau B.K., "Design of multi-antenna feeding for MIMO terminals based on characteristic modes", IEEE Antennas and Propagation Society International Symposium (APS), 2013, pages 182-183.

[16] Miers Z., Li H., Lau B.K., "Design of bandwidth enhanced and multiband MIMO antennas using characteristic modes", IEEE Antennas and Wireless Propagation Letters, 2013, pages 1696-1699.

[17] Grieg D.D., Engelmann H.F., "Microstrip - a new transmission technique for the kilomegacycle range", Proceedings of the IRE, volume 40, 1952, pages 1644-1650.

[18] CSTworld, Webinars, "Reconfigurable antenna simulation", 2012, accessed Oct. 2015: https://www.youtube.com/watch?v=oTSsFJ35YVQ/

[19] Safin E., Mantueffel D., "Reconstruction of the characteristic modes on an antenna based on the radiated far field", IEEE Transactions on Antennas and Propagation, 2013, pages 2964-2971.

[20] Li H., Miers Z., Lau B.K., "Design of orthogonal MIMO handset antennas based on characteristic mode manipulation at frequency bands below 1 GHz", IEEE Transactions on Antennas and Propagation, volume:62, 2014, pages 2756-2766.

[21] Das S.K., *Mobile Handset Design*, John Wiley & Sons, 2010, ISBN 978-0-470-82467-2.

[22] Taga T., Tsunekawa K., "Performance analysis of a built-in planar inverted F antenna", IEEE Journal on Selected Areas in Communications, volume:5, 1987, pages 921-929.

[23] Rodrigo D., Cetiner B.A., Jofre L., "Frequency, radiation pattern and polarization reconfigurable antenna using a parasitic pixel layer", IEEE Transactions on Antennas and Propagation, volume:62, 2014, pages 3422-3427.

[24] Miers Z., Li H., Lau B.K., "Design of bezel antennas for multiband MIMO terminals using characteristic modes". European Conference on Antennas and Propagation (EuCAP), 2014, pages 2556-2560.

[25] Zhu J., Eleftheriades C.V., "A simple approach for reducing mutual coupling in two closely spaced metamaterial-inspired monopole antennas", IEEE Antennas Wireless Propagation Letters, volume: 9, 2010, pages 379-382.

List of Acronyms

CM	Characteristic Mode
CPU	Central Processing Unit
CST	Computer Simulation Technology
DGS	Defected Ground Structure
EM	Electromagnetic
IFA	Inverted-F Antenna
LTE	Long Term Evolution
LTE-A	Long Term Evolution Advanced
MIMO	Multiple-Input Multiple-Output
MOM	Method of Moments
PIFA	Planar Inverted-F Antenna
SAR	Specific Absorption Rate
TCM	Theory of Characteristic Modes